ACS OMEGA

http://pubs.acs.org/journal/acsodf

Article

Size-Dependent Catalytic Activity of PVA-Stabilized Palladium Nanoparticles in *p*-Nitrophenol Reduction: Using a Thermoresponsive Nanoreactor

Sujit Chatterjee and Swapan Kumar Bhattacharya*

Cite This: *ACS Omega* 2021, 6, 20746−20757

Read Online

ACCESS | Metrics & More | Article Recommendations | Supporting Information

ABSTRACT: Palladium nanoparticles (Pd NPs) of various average global diameters (2.1−7.1 nm) encapsulated with hydrophilic polymer polyvinyl alcohol (PVA) have been synthesized and used as catalysts for sodium borohydride assisted reduction of *p*-nitrophenol to *p*-aminophenol. The synthesized catalysts exhibit excellent and typical size-dependent catalytic activity in the green protocol. UV−visible absorption spectroscopy, X-ray diffraction, scanning electron microscopy, and transmission electron microscopy were employed to characterize the prepared Pd NPs. The kinetics of this reaction was easily monitored by a UV−visible absorption spectrophotometer. The mechanism of the reaction is explained by the Langmuir−Hinshelwood model. The catalytic performance increases with decreasing size of the synthesized nanoparticles. The apparent rate constants ($k_{app} \times 10^3/s^{-1}$) of the catalytic reduction in the presence of Pd NPs of average diameters of 2.1, 3.35, 6.2, and 7.1 nm are determined as 8.57, 7.67, 6.16, and 5.04, respectively, at 298 K by using 2.91 mol % palladium nanocatalyst in each case. Moreover, the estimated activation energy of 22.2 kJ mol^{-1} obtained for Pd NPs with the smallest average diameter of 2.1 nm is very low as reported in the literature for the reduction. The influences of catalyst dose and concentration of *p*-nitrophenol on catalytic reduction are fully investigated. The catalyst with the largest diameter shows a temperature-sensitive property that might be due to the presence of a very low amount of rapped PVA used as stabilizer during the fabrication process. Thus, the synthetic protocol provides a unique fabrication process of a catalytically active thermoresponsive nanoreactor consisting of Pd NPs encapsulated into a PVA stabilizing agent.

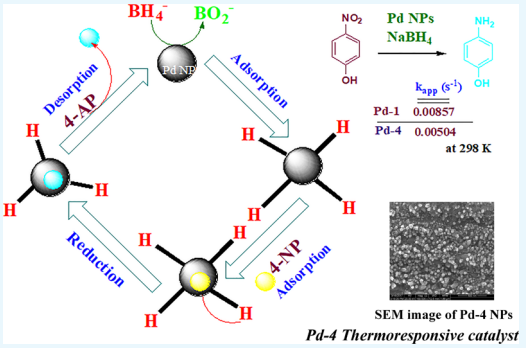

INTRODUCTION

In the past few decades, ultrafine noble metal nanoparticles like Pt, Pd, etc., have been extensively studied due to their high surface area; high surface to volume ratio; catalytic capability; and excellent mechanical, chemical, and thermal robustness.[1−3] Due to the outstanding catalytic activity, Pd nanoparticles (Pd NPs) have been advocated as one of the most promising candidates of the catalysis for a long time.[4−8] These nanoparticles are mainly used in heterogeneous catalysis, for example, coupling, dehalogenation, and reduction reactions. However, the major drawback of ultrafine NPs is that they can easily aggregate due to their high surface energy. There are a large number of templates that have been developed and employed by researchers for a better catalytic performance of metal nanoparticles by decreasing agglomeration and thus increasing reusability,[9] for example, polymers, dendrimers, micelles, peptides, metal−organic frameworks (MOFs), carbon materials, graphene, metal oxides, ionic liquids, and porous silica.[10−20] Therefore, Pd NPs stabilized by suitable templates with advanced catalytic activity have attracted growing attention owing to their unique properties and great potential in the field of catalysis.[21] Lu and co-workers reported thioether-containing covalent organic framework (PtNPs@COF and PdNPs@COF) nanocomposites that showed excellent catalytic activities toward Suzuki−Miyaura coupling reactions and reduction of *p*-nitrophenol (*p*-NP) under an ambient condition. Moreover, these COF-template-supported ultrafine nanocomposites are highly stable and reusable without loss of catalytic activity.[14] Poly(amido)amine (PAMAM) dendrimer supported palladium nanoparticles showed remarkable size-dependent catalytic activities toward the reduction of *p*-nitrophenol by $NaBH_4$ in an aqueous solution.[11] Nowadays, the reduction of *p*-nitrophenol to *p*-aminophenol by borohydride ions (BH_4^-) is considered as a model reaction to investigate the relative catalytic activities of several nanoparticles.[22] This reaction can be easily monitored with high precision by UV−vis spectroscopy by the decrease of

Received: February 18, 2021
Accepted: May 31, 2021
Published: August 6, 2021

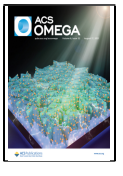

https://doi.org/10.1021/acsomega.1c00896
ACS Omega 2021, 6, 20746−20757

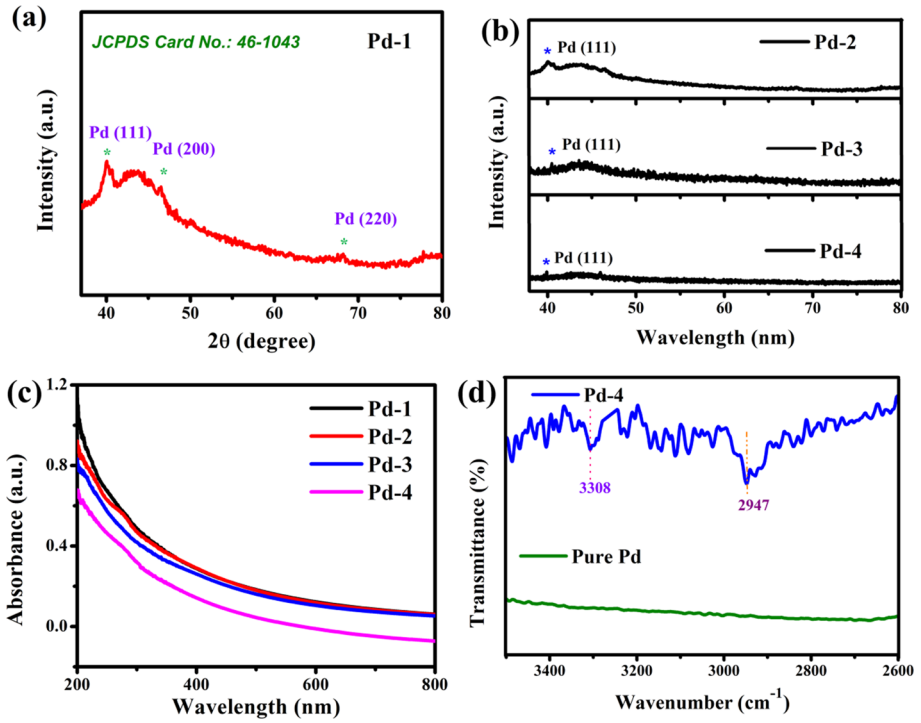

Figure 1. XRD pattern of Pd(0) nanoparticles of (a) Pd-1 and (b) Pd-2, Pd-3, and Pd-4 (in the presence of activated charcoal powder); (c) the UV−visible spectra of 10 times diluted aqueous solution of Pd-1, Pd-2, Pd-3, and Pd-4 catalysts; and (d) the FT-IR spectra of Pd-4 (blue line) and pure Pd (green line).

absorbance of *p*-nitrophenolate anion at 400 nm.[23] The presence of isosbestic points in the UV−vis absorption spectra for the reduction of *p*-nitrophenol by $NaBH_4$ in the presence of nanocatalysts reveals that *p*-nitrophenol is completely reduced to *p*-aminophenol, and no byproducts can be detected.[24]

In recent years, great efforts have been devoted to fabricating various temperature-sensitive hydrogel materials due to their potential application in medicinal chemistry as well as in catalysis for a large number of reactions.[25−28] The fabrication of a temperature-sensitive hydrogel (nanoreactor) is mainly achieved by using a suitable hydrophilic template.[29,30] Recently, poly(*N*-isopropylacrylamide) was extensively used to prepare such kind of novel "smart" materials that exhibit volume phase transition in response to environmental stimuli, like temperature, pH, etc., by utilizing its semi-interpenetrating polymeric networks.[31] Although PVA possesses the same type of polymeric networks, the fabrication of thermosensitive hydrogels is very rare. L. Tzounis and co-workers synthesized an efficient thermoresponsive nanoreactor, the AuAg@pNIPAM@Ag hybrid microgel, by using poly(*N*-isopropylacrylamide) (pNIPAM) microgels as templates, which showed excellent catalytic activity toward *p*-nitrophenol reduction reaction by using sodium borohydride as the reductant.[32] R. Begum and co-workers synthesized a polymer-based nanoreactor, Ag-p(NIPAAm-HEMA-AAc), for the catalytic reduction of *p*-nitrophenol by using poly(*N*-isopropyl acryl amide-2-hydroxy methyl methacrylate-acrylic acid) (p-NIPAAm-HEMA-AAc) polymer microgels. This group synthesized this polymer by free-radical emulsion polymerization using *N*-isopropyl acrylamide as the main monomer. This nanoreactor was prepared in a multistep method by the reduction of silver ions by $NaBH_4$ within the framework of initially synthesized (pNIPAM) microgels.[33]

Here we demonstrate a full kinetic analysis based on the Langmuir−Hinshelwood model of the reduction of *p*-nitrophenol by $NaBH_4$ in the presence of Pd NPs of various dimensions.[34,35] According to the model, both *p*-NP and hydrogen are chemisorbed on the surface of Pd NPs before the reduction reaction takes place. Moreover, the influence of catalyst dose, $NaBH_4$ concentration, and *p*-nitrophenol concentration on the reduction of *p*-nitrophenol was investigated by using a superior Pd nanocatalyst. The PVA-embedded Pd NPs showed remarkable size-dependent catalytic activity toward the reduction of the hazardous nonbiodegradable organic pollutant *p*-nitrophenol, with superior catalytic activity of as-synthesized Pd NPs with the smallest dimensions compared to that of larger ones owing to their large surface areas.[35] Herein, we also report that the PVA-supported Pd NPs with larger dimensions, denoted as Pd-4, can exhibit properties like a thermoresponsive nanoreactor.

RESULTS AND DISCUSSION

Characterization. Figure 1a,b exhibits the representative XRD patterns of Pd NPs in the synthesized materials Pd-1−4. Three characteristic peaks at the 2θ values of 40.1, 46.6, and 68.1° correspond to the (111), (200), and (220) diffraction planes of the face-centered cubic (fcc) Pd (JCPDS Card No. 46-1043). Moreover, there is a broad diffraction peak around 44.5° corresponding to the (101) plane of the hexagonal primitive lattice of graphite carbon (JCPDS Card No. 89-8487). The PXRD patterns of other sets of synthesized nanocatalysts that are Pd-2, Pd-3, and Pd-4 depict the (111) plane of fcc Pd at 2θ value of 40.01° as presented in Figure 1b.

Figure 1c shows the typical UV−vis absorption spectra of as-synthesized Pd NPs in Pd-1, Pd-2, Pd-3, and Pd-4 nanocatalysts. The absence of a peak for the metal to ligand charge transfer complex in as-synthesized nanoparticles reveals the

https://doi.org/10.1021/acsomega.1c00896
ACS Omega 2021, 6, 20746−20757

complete reduction of Pd^{2+} ions and the formation of Pd (0) NPs. The intensity of absorption spectra of as-prepared PVA-embedded Pd nanocatalysts decreases with increasing diameter of Pd nanoparticles.[3] Therefore, it demonstrates that the average diameter of Pd nanoparticles follows the following sequence: Pd-1 < Pd-2 < Pd-3 < Pd-4.

Figure 1d shows the FT-IR spectra of the as-synthesized Pd-4 nanocatalyst and the pure Pd. The FT-IR studies of Pd-4 show two broad absorption peaks at 3308 and 2947 cm^{-1}, which are mainly due to the O−H and C−H stretching, respectively. On the other hand, these kinds of stretching are completely absent in the case of the pure Pd prepared without PVA. Thus, this result demonstrates that Pd NPs are wrapped by PVA in Pd-4 to form a nanoreactor.[36]

The scanning electron microscope (SEM) images of Pd-1 and Pd-4 and of Pd-2 and Pd-3 are shown in Figure 2a,b and

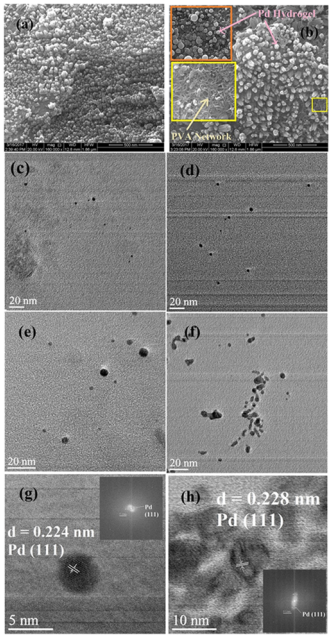

Figure 2. SEM images of Pd NPs of (a) Pd-1 and (b) Pd-4 (inset manifests the PVA hydrogel encapsulated Pd NPs). The inset with yellow border shows semi-interpenetrating polymeric networks composed of PVA of Pd-4. The TEM images of (c) Pd-1, (d) Pd-2, (e) Pd-3, and (f) Pd-4 and HRTEM images of (g) Pd-1 and (h) Pd-4 nanocatalysts (inset showing SAED patterns), respectively.

Figure S1 (in the Supporting Information), respectively. It was observed that all the as-synthesized Pd NPs have a uniform spherical morphology.[3] As shown in the inset of Figure 2b, numerous ultrafine hydrogels of Pd NPs in Pd-4 are highly dispersed.

The TEM images of Pd-1, Pd-2, Pd-3, and Pd-4 are shown in Figures 2c−f, respectively. Figure S2 reveals that the mean diameters (nm) of as-synthesized Pd NPs from several TEM micrographs of each sample of Pd-1, Pd-2, Pd-3, and Pd-4 are 2.1, 3.35, 6.2, and 7.1, respectively. Figure 2g,h shows the high-resolution TEM images of Pd-1 and Pd-4 nanocatalysts, respectively, in spite of the SAED patterns of Pd NPs in Pd-1 and Pd-4 present at the inset of Figure 2g,h, respectively. The interplanar crystal spacing of 0.228 nm corresponds to the (111) plane of face-centered cubic (fcc) Pd (JCPDS Card No. 87-0641). The TEM and HRTEM images also reveal that the shape of as-synthesized Pd NPs is almost spherical.

Catalytic Studies. The present study aimed to investigate the catalytic activity of as-synthesized Pd NPs toward *p*-nitrophenol reduction reaction by using $NaBH_4$ as a reducing agent in an aqueous solution. According to the Langmuir−Hinshelwood kinetic model, the adsorption of *p*-nitrophenolate ions and active hydrogen on the metal nanoparticles is reversible and assumed to be very fast (Scheme 1). A

Scheme 1. Mechanistic Model of the Langmuir−Hinshelwood Mechanism for the Reduction of *p*-Nitrophenol to *p*-Aminophenol by Sodium Borohydride in the Presence of Pd NPs in Aqueous Solution

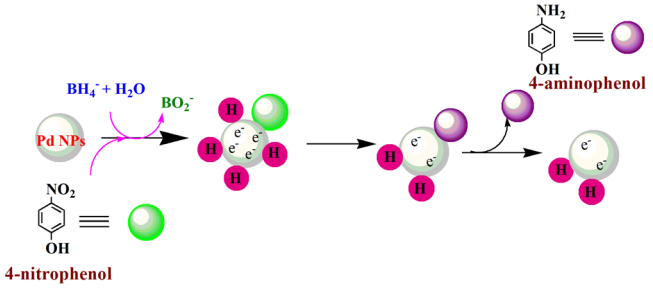

mechanistic study reveals that *p*-nitrophenol is first quickly reduced to *p*-nitrosophenol and then to a stable intermediate, *p*-hydroxyl aminophenol, and finally, *p*-hydroxyl aminophenol is reduced to the final product, *p*-aminophenol, and detached from the metal surface, thus creating a free surface, and the catalytic cycle starts again. This final step is the rate-determining step.[39−41]

Figure 3 shows the UV−vis spectra of *p*-nitrophenol in the absence and presence of $NaBH_4$. As can be seen in Figure 3,

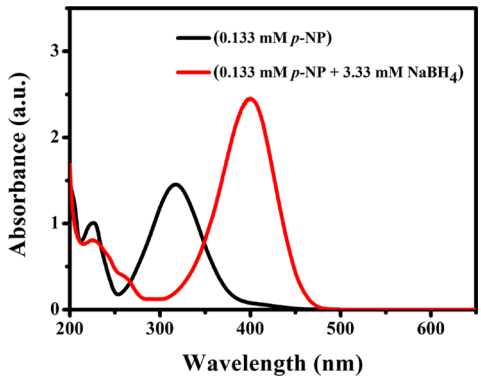

Figure 3. UV−vis absorption spectra of 0.133 mM *p*-nitrophenol in the absence of $NaBH_4$ and in the presence of 3.33 mM $NaBH_4$.

the aqueous solution of *p*-NP shows a maximum absorption (λ_{max}) at 320 nm. In the presence of $NaBH_4$, the light yellow solution of aqueous *p*-nitrophenol turns immediately to yellow (λ_{max} at 400 nm), demonstrating the production of *p*-nitrophenolate anion. The progress of the hydrogenation reaction is easily monitored kinetically by UV−vis spectroscopy. With increasing reaction times, the main peak of the *p*-nitrophenolate ion at 400 nm decreases, while a new peak of *p*-aminophenolate ions appears at 300 nm and gradually increases with increasing reaction time until complete reduction. The presence of several isosbestic points in the UV−vis spectra of the reaction mixture indicates that there is no side reaction occurring in this reaction. The kinetic

https://doi.org/10.1021/acsomega.1c00896
ACS Omega 2021, 6, 20746−20757

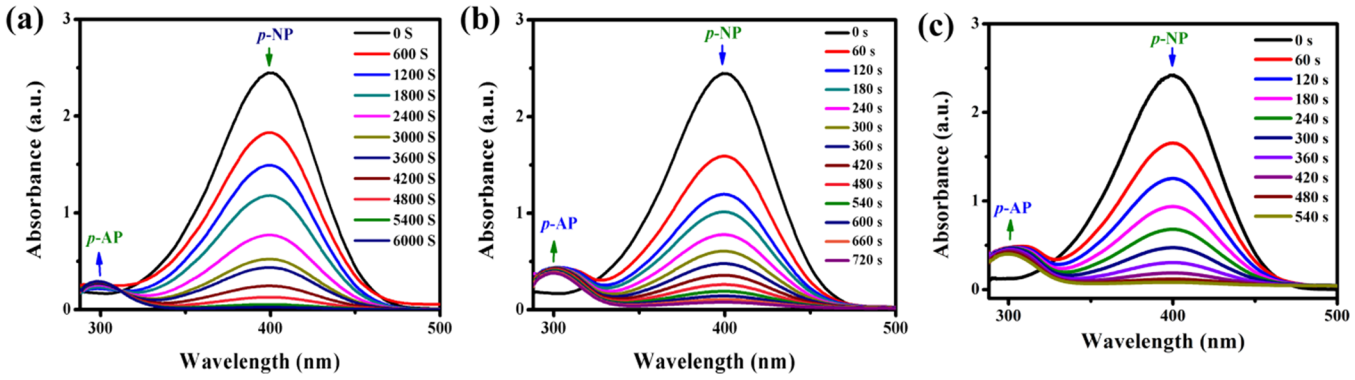

Figure 4. Time-dependent UV−vis absorption spectra for the reduction of *p*-NP in the presence of different amounts of catalyst Pd-1: (a) 2 μL, (b) 11 μL, and (c) 22 μL. Reaction conditions: [*p*-NP] = 0.133 mM, [$NaBH_4$] = 3.33 mM, and T = 293 K.

equation for the catalytic reduction of *p*-nitrophenol to *p*-aminophenol in the presence of excess $NaBH_4$ in aqueous solution by Pd NPs can be written as eq 1:

$$\ln\left(\frac{A_t}{A_0}\right) = -k_{app} \times t \tag{1}$$

where k_{app} is the apparent rate constant and A_t and A_0 are the absorbance of *p*-NP at time t and the initial stage, respectively.

The catalyst loading effect of Pd-1 NPs on the reduction of the *p*-nitrophenolate ion was tested at 293 K using eq 1. As shown in Figure 4, the intensity of the *p*-nitrophenolate ion gradually decreases with time, and a new peak at 300 nm corresponding to the peak of *p*-aminophenol appeared in each case of a different amount of Pd-1 loading. Figure 4a−c displays the profiles for catalyst loading of 2, 11, and 22 μL, respectively.

Table 1 reveals that the time required for 98% conversion of *p*-nitrophenol to *p*-aminophenol decreases with the increasing amount of the catalyst in the reaction mixture, keeping all other variables constant. This is mainly due to the increase in the available active sites for the reactants to adsorb on the surface of the Pd-1 catalyst.[45] Moreover, after 12 min, the absorption peak of *p*-NP at 400 nm completely disappeared by using 11 μL of the Pd-1 catalyst as shown in Figure 4b, whereas the time required for the complete reduction of *p*-NP by using 2 and 22 μL of the Pd-1 catalyst was 100 and 9 min, respectively, implying that 11 μL of Pd-1 is the ideal amount of catalytic precursor in this reaction mixture.

Table 1. The Effect of Catalyst (Pd-1) Loading on the Catalytic Reduction of *p*-NP by $NaBH_4$ in Aqueous Solution[a]

amount of catalyst (μL)	[concentration of the catalyst Pd(0) in the reaction mixture (M)]×10^7	time (min) required for 98% conversion	percentage conversion (% E) at 6 min
2	7.47	90	16
11	41.07	11	81
22	82.13	9.0	87

[a]Reaction conditions: concentrations of *p*-nitrophenol and $NaBH_4$ in the reaction cuvette were 0.133 and 3.33 mM, respectively. The reaction temperature (T) was 293 K.

The pseudo-first-order rate constant (k_{app}) at an ambient temperature using the optimum amount of catalyst in the reaction mixture was calculated from the slope of the plot of $\ln(A_t/A_0)$ versus reaction time t (s). The value of k_{app} ($s^{-1} \times 10^3$) at 25 °C was obtained as 8.57, 7.67, 6.16, and 5.04 for Pd-1, Pd-2, Pd-3, and Pd-4 nanocatalysts, respectively. It clearly reveals that the catalytic activity decreases with the increasing diameter of as-synthesized globule Pd nanoparticles, which indicates the typical size-dependent catalytic activity of Pd NPs.[21] The obtained normalized rate constant (k_{nor}) value of Pd-1 at 25 °C was 695.6 × 10^3 s^{-1} mol^{-1-1} ($k_{nor} = k_{app}/n$, where n is the number of moles of Pd in the reaction curette). The percentage conversion efficiency (%E) of as-synthesized Pd NPs of various diameters for the catalytic reduction of *p*-nitrophenol by $NaBH_4$ in aqueous solution was calculated using eq 2 (Table 1):

$$\%E = \frac{(C_0 - C_t)}{C_0} \times 100 \tag{2}$$

where C_t is the concentration of *p*-NP measured at time t and C_0 is the initial concentration of *p*-NP measured at time zero.

After the reduction of *p*-nitrophenol by $NaBH_4$ in the presence of Pd NPs, the yellow color of the *p*-nitrophenolate solution changed to colorless, which can be precisely monitored by UV−vis spectroscopy. Figure 5a,b shows the time-dependent UV−vis spectra of *p*-NP at 25 °C in the presence of Pd-1 and Pd-4 nanocatalysts [41.07 × 10^{-7}M Pd(0) in 3 mL of the reaction mixture in the cuvette], respectively.[42,43] As shown in Figure 5a,b, the absorption peak of the *p*-nitrophenolate ion at 400 nm gradually decreases during the reaction, while the concomitant peak of *p*-aminophenol at near 300 nm gradually increases, indicating that the *p*-NP could be reduced to *p*-AP by $NaBH_4$ in the presence of Pd NPs. Moreover, the time required for the complete reduction of *p*-NP, i.e., for the complete disappearance of the peak for the *p*-nitrophenolate ion, by Pd-1 and Pd-4 is found to be 8 and 14 min, respectively. Therefore, it can be concluded that the catalytic efficiency of the Pd-1 nanocatalyst is greater than that of Pd-4 since Pd-1 consists of Pd NPs of smaller dimension and greater surface area; as a result, it provides more active sites for reduction.[44]

The influence of the concentration of *p*-nitrophenol on k_{app} of this reduction reaction in the presence of the Pd-1 nanocatalyst is shown in Figure 6. Figure 6a represents the $\ln(A_t/A_0)$ versus reaction times at different concentrations of *p*-nitrophenol using Pd-1 as the catalyst at 298 K temperature. From the slope of the fitted line, the apparent rate constant (k_{app}) was determined. Figure 6b shows the k_{app} values as a function of the concentrations of *p*-nitrophenol in the reaction

https://doi.org/10.1021/acsomega.1c00896
ACS Omega 2021, 6, 20746−20757

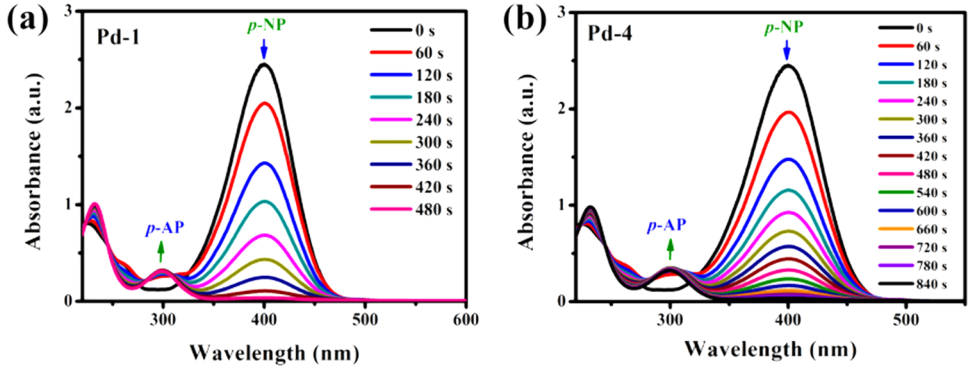

Figure 5. UV−vis absorption spectra of the gradual reduction of *p*-NP by using $NaBH_4$ in the presence of (a) Pd-1 and (b) Pd-4 nanocatalysts. Reaction conditions: [*p*-NP] = 0.133 mM, [$NaBH_4$] = 3.33 mM, [Pd] = 41.07 × 10^{-7} M, *T* = 298 K.

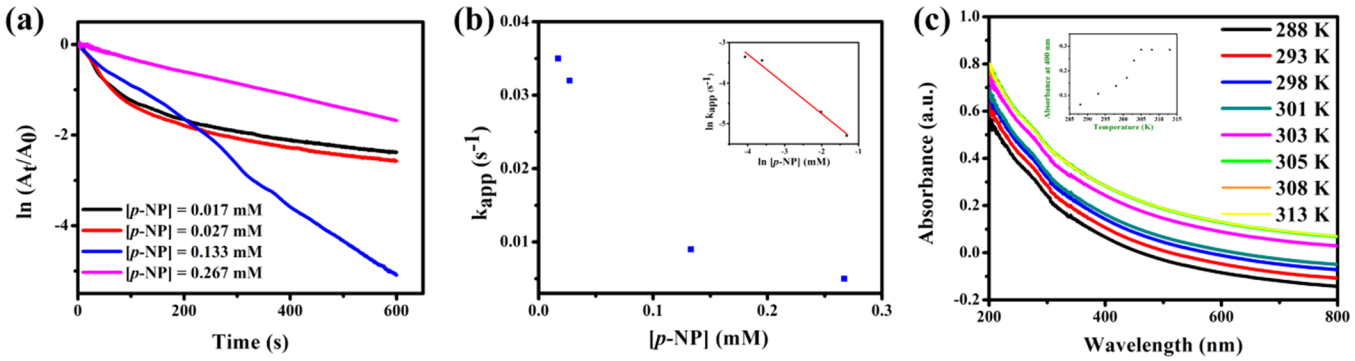

Figure 6. (a) Kinetic plot of $\ln(A_t/A_0)$ versus reaction time for the reduction of *p*-nitrophenol by $NaBH_4$ in the presence of the Pd-1 nanocatalyst at 298 K using different concentrations of *p*-nitrophenol. (b) The plot of k_{app} (s^{-1}) versus the concentration of *p*-nitrophenol (in mM) in the reaction cuvette (with the inset showing ln k_{app} versus ln[4-NP] plot). (c) The typical UV−vis spectra of 10 times dilute stock solution of the catalyst Pd-4 at different temperatures exhibit nanoreactor properties (inset shows the absorbance of Pd-4 at 400 nm versus the temperature plot).

mixture for Pd-1 nanocatalysts (Table 2). These results indicate that the apparent rate constant decreases significantly

Table 2. Influence of the Concentration of *p*-Nitrophenol on the Apparent Rate Constant of the Catalytic Reduction of *p*-Nitrophenol by $NaBH_4$ as the Reducing Agent in the Presence of the Pd-1 Catalyst[a]

concentration of the *p*-nitrophenol in the reaction mixture (mM)	k_{app} (s^{-1})
0.017	0.035
0.027	0.032
0.133	0.009
0.267	0.005

[a]Reaction conditions: [$NaBH_4$] = 3.33 mM, [Pd] = 41.07 × 10^{-7} M, and *T* = 298 K.

with the increasing concentration of *p*-nitrophenol due to a decrease in the effective number of active sites of the Pd NPs for adsorption of reactive hydrogen at ambient temperature. Therefore, it is concluded that the apparent rate constant is proportional to the total available surface area of metal nanoparticles. Figures 6a,b shows the dependence of the rate constant on the concentration of *p*-nitrophenol for the reduction of *p*-nitrophenol in the presence of the Pd-1 nanocatalyst at 298 K temperature, with the inset showing ln k_{app} versus ln[4-NP] plot (Table 2). The linear fit of ln k_{app} versus ln[4-NP] with a slope of nearly 1 implies that the rate constant decreases linearly with the first order of concentration of *p*-nitrophenol.

For evaluating the kinetic parameters of our as-synthesized PVA-embedded Pd nanocatalysts, the reduction of *p*-nitrophenol was carried out at different temperatures as shown in Figure S3 by using 41.07 × 10^{-7} M Pd nanocatalysts in a reaction cuvette in each experiment.[46] The apparent rate constants (k_{app}) at different temperatures were calculated from the linear portion of $\ln(A_t/A_0)$ versus the reaction time plot at each temperature. The rate constant is considered as apparent since previously reported works of many groups have shown that the observed rate constant depends on the concentration of $NaBH_4$ as well as the concentration of *p*-nitrophenol. The values of apparent rate constants at different temperatures for Pd-1, Pd-2, Pd-3, and Pd-4 nanocatalysts are listed in Table S1 in the Supporting Information, illustrating that, for Pd-1, the rate constant gradually increases with temperature from 6.5 × 10^{-3} s^{-1} at 288 K to 2.44 × 10^{-2} s^{-1} at 323 K due to the faster molecular motion and greater chance of the collision and then it decreases sharply with increasing temperature up to 333 K due to the extent of adsorption of *p*-NP and hydrogen decreases at the higher temperature. On the other hand, in the case of Pd-2 and Pd-3, the rate constant is increased with temperature from 288 to 328 K; then, on further increasing the temperature, the rate constant remains unchanged, indicating compensation of increased collision by less adsorption at the higher temperature. For Pd-4, the rate constant increases linearly from 2.07 × 10^{-3} s^{-1} at 288 K to 7.37 × 10^{-3} s^{-1} at 303 K, showing similarity with Pd-1, Pd-2, and Pd-3 up to 303 K. After that, it decreases with increasing temperature up to 5.04 × 10^{-3} s^{-1} at 318 K and then again increases with

https://doi.org/10.1021/acsomega.1c00896
ACS Omega 2021, 6, 20746−20757

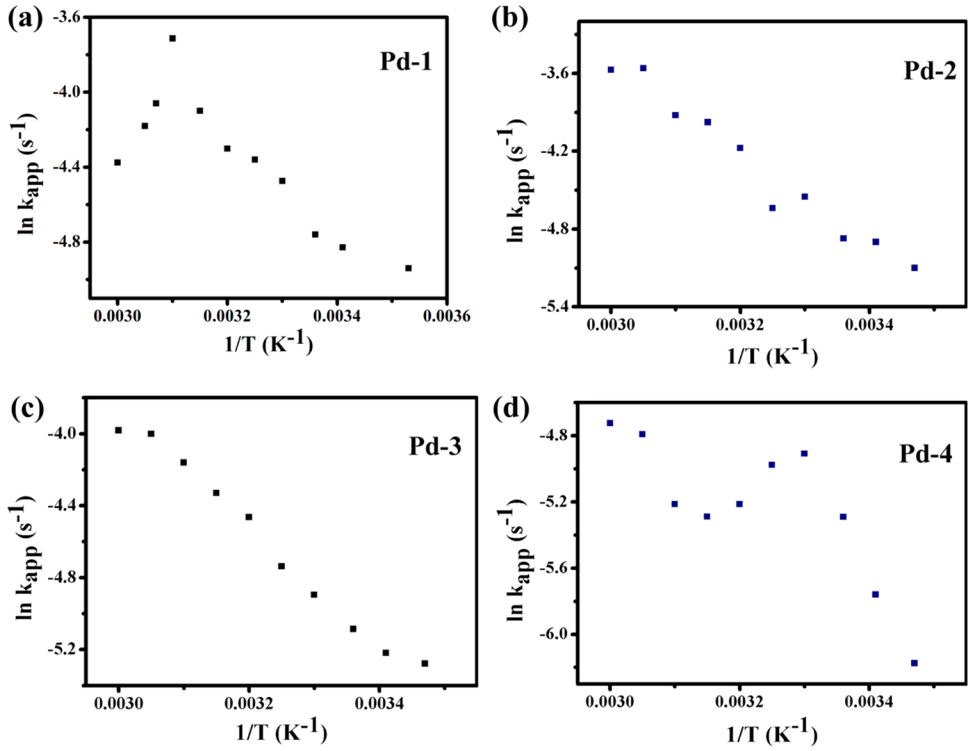

Figure 7. The plot of ln k_{app} versus $1/T$ for 4-nitrophenol reduction at different temperatures in the presence of (a) Pd-1, (b) Pd-2, (c) Pd-3, and (d) Pd-4 nanocatalysts. Reaction conditions: [*p*-NP] = 0.133 mM, [$NaBH_4$] = 3.33 mM, and [Pd] = 41.07 × 10^{-7} M.

increasing temperature up to 8.92 × 10^{-3} s^{-1} at 333 K, exhibiting the typical behavior of a nanoreactor (temperature-sensitive hydrogel). This has occurred when the particle dimension of Pd is relatively large and hence the adsorption layer of PVA is also relatively less thick. For the preparation of this particle, a very low amount of PVA is used as a hydrophilic capping agent for the synthesis of Pd-4 NPs illustrated by UV−vis spectra of Pd-4 at different temperatures as shown in Figure 6c.[47] A plot of absorbance versus temperature (at the inset of Figure 6c) reveals an increase of absorbance up to 305 K, beyond which it attains a steady value indicating phase transition due to the removal of water. In catalyst Pd-4, a recognizable bonding interaction is observed. Since the Pd NPs in Pd-4 are stabilized by the little amount of PVA (containing both hydrophobic and hydrophilic parts), the hydrophobic carbon−carbon skeleton of PVA approaches toward the uncharged spherical palladium nanoparticle, and the hydrophilic OH groups of PVA flank toward the polar water molecules at any temperature. At low temperature, the movement of water molecules due to Brownian motion is quite slow, and thus, these behave comparatively more static than at high temperature, and thus, the surrounding water molecules about PVA-embedded Pd NPs are capable of forming a greater number of hydrogen bonds with the hydroxyl (OH) groups of PVA along with hydrogen bonds themselves at a very low temperature. As a result, the PVA layer around Pd NPs is shifted toward surrounding water molecules (hydrophilic solvent), but with increasing temperature, the surrounding water molecules move faster, and thus, the intermolecular hydrogen bonds between PVA and surrounding water molecules are elongated and few of them are collapsed, which facilitate the approaching of the PVA layer toward the palladium nanoparticle since London forces between the spherical palladium and PVA increase with decreasing distance that becomes maximum at 32 °C, probably due to destroying of the maximum number of possible intermolecular hydrogen bonds between the OH groups of PVA (hydrophilic polymeric network) and surrounding water molecules. This might be due to the intermolecular hydrogen bonds between the same species being much greater than those between different species. Since this temperature is irrespective of the nature of the hydrophilic polymer framework in hydrogels, it might be a distinct property of water molecules. Therefore, above 32 °C, the catalytic activity of the as-prepared PVA-encapsulated Pd nanoparticles (Pd-4) is reduced because of the shrinkage of hydrophilic PVA networks. On the other hand, UV−vis spectra of Pd-1 at different temperatures demonstrate that the size of the Pd NPs in Pd-1 remains unchanged at the temperature range of 288 to 313 K as shown in Figure S4. This is mainly due to the presence of a thicker layer of PVA around smaller-sized nanoparticles since a large amount of PVA is used during the synthesis of Pd-1. Thus, Figure S4 reveals that Pd-1 cannot behave as a thermoresponsive nanoreactor.

The activation energy of the reaction in the presence of as-synthesized Pd NPs was calculated by using the Arrhenius equation (eq 3):

$$\ln k_{app} = -\frac{E_a}{R}\cdot\frac{1}{T} + \ln A \tag{3}$$

where E_a is the activation energy, R is the universal gas constant, and A is the pre-exponential factor. From the apparent rate constants at four different temperatures (at the lower-temperature region), we have determined the activation energy of this reduction reaction (Figure 7).

A linear relationship between ln k_{app} and the reciprocal of temperature was found for catalysts Pd-1, Pd-2, and Pd-3 from which we determined the activation energy of this reaction (Table S2). But in the case of Pd-4, a nonlinear Arrhenius

https://doi.org/10.1021/acsomega.1c00896
ACS Omega 2021, 6, 20746−20757

relation was found since the little amount of hydrophilic PVA-stabilized Pd NPs behaves as a temperature-sensitive hydrogel; hence, the activity of this catalyst on *p*-nitrophenol reduction reaction is controlled by diffusion. In contrast, the reduction reaction is not controlled by diffusion in the case of Pd-1, Pd-2, and Pd-3 nanocatalysts. Thus, the support plays a crucial role to determine the catalytic activity of metal nanoparticles. At very low temperatures of about 15 °C, thin PVA networks in Pd-4 swell by the uptake of water molecules from the reaction medium, which facilitates the diffusion of the reactants up to the surface of the nanocatalyst through the PVA network. Raising the temperature above ca. 303 K leads to a phase transition in which the water is gradually expelled.[48] When the reaction temperature is 305 K, the water molecules are almost expelled from the catalyst surface, causing maximum absorbance at the temperature. Above 305 K (32 °C), the microgel shell shrank markedly followed by the concurrent slowing down of the diffusion of reactants within the network. This in turn decreases the rate constant (k_{app}) catalyzed by the metal nanoparticles immobilized in microgels. Thus, the rate constant, k_{app}, reaches its minimum value at the transition temperature of 318 K. Above this temperature, the microgel is gradually removed from the nanoparticle surface due to the increased kinetic energy of the molecules. Thus, the rate constants are again increased from that temperature. The value of activation energy (E_a) for the catalytic reduction of *p*-nitrophenol by Pd-1, Pd-2, Pd-3, and Pd-4 nanocatalysts is 22.2, 29.2, 26.2, and 63.22 kJ mol^{-1}, respectively, as shown in Table 3. Notably, for the measurement of E_a of the Pd-4 catalyzed reaction, only initial temperatures ranging from 288 to 303 K are considered. It is expected that the activation energy of this reaction would be a function of the size of the Pd NPs, but it may also depend on other factors and not strictly on the size of NPs.[44] Moreover, the activation parameters like the enthalpy of activation ($\Delta H^{\#}$) and entropy of activation ($\Delta S^{\#}$) are calculated by using the Eyring equation (eq 4):[49]

Table 3. Summary of the Activation Energy, Enthalpy, Entropy, and k_{app} per Unit Surface Area of the Synthesized Nanoparticles for the Reduction of *p*-Nitrophenol by Pd-1, Pd-2, Pd-3, and Pd-4 Nanocatalysts

catalyst	Pd-1	Pd-2	Pd-3	Pd-4
E_a (kJ mol^{-1})	22.2	29.2	26.02	63.22
$\Delta H^{\#}$ (kJ mol^{-1})	19.73	26.61	23.47	60.72
$\Delta S^{\#}$ (J mol^{-1} K^{-1})	−217.5	−195.3	−207.8	−84.90
k_{app}/S (s^{-1} cm^{-2})	7042	4415	2385	2083

$$\ln\left(\frac{k_{app}}{T}\right) = \ln\left(\frac{k_B}{h}\right) + \frac{\Delta S^{\neq}}{R} - \frac{\Delta H^{\neq}}{R}\left(\frac{1}{T}\right) \quad (4)$$

where k_B is the Boltzmann constant (1.38×10^{-23} J K^{-1}) and h is the Plank's constant (6.626×10^{-34} J s). By plotting $\ln(k_{app}/T)$ versus $(1/T)$, the values of entropy of activation and enthalpy of activation are evaluated from the intercept and slope by considering the k_{app} value of at least four different temperatures starting from 288 K as shown in Figure 8 (Table S3). Table 3 implies that the $\Delta H^{\#}$ of Pd-1 is the least positive magnitude and that of Pd-4 is the highest positive magnitude, whereas $\Delta S^{\#}$ is the largest negative value for Pd-1 and the least negative value for Pd-4. This indicates the presence of the associative reaction step revealing a transition state.[50]

A plot of the logarithm of frequency factor (log A) versus the apparent activation energy, E_a, is a straight line exhibiting the inherent consequence of the compensation law of the Langmuir−Hinshelwood mechanism, independent of dimension and protecting layer thickness of nanocatalysts (Figure 9). Notably, the linear increase of log A with the apparent activation energy observed might be due to the decrease of the adsorption affinity (increase of enthalpy) and/or the thickness of the protecting layer around the nanocatalysts.

To get a direct proof of the presence of more active sites in Pd-1 in comparison to the other synthesized catalysts, the surface area (S) of the synthesized nanoparticles is determined by using the equation $S = 6\ m/d\rho$, where d, m, and ρ are the average diameter, mass, and density of the synthesized nanoparticles. A comparison of the apparent rate constants per unit surface area (k_{app}/S) of the synthesized nanoparticles presented in Table 3 reveals the order Pd-1 > Pd-2 > Pd-3 > Pd-4 among the synthesized catalysts. This can be considered as a direct proof of the presence of more active sites on Pd-1.

To demonstrate the significant advantages of our synthesized catalyst for the reduction of *p*-nitrophenol by $NaBH_4$, the performance of the different catalysts reported in the literature is reported in Table 4 for comparison. The outcome shows that Pd-1 is a more efficient catalyst considering the apparent rate constants of all the catalysts. Therefore, it is concluded that the Pd NPs with smaller dimensions exhibit better catalytic performance toward *p*-nitrophenol reduction reaction.[56]

The morphologies of the PVA-embedded Pd hydrogels (Pd-4) are shown in the inset of Figure 2b, which exhibits the honeycomb structure of the PVA polymer consisting Pd NPs.[31] Moreover, the inset of Figure 2b also reveals that the semi-interpenetrating polymeric networks of PVA facilitate the formation of distinct nanoreactor properties.

Stability is a crucial factor in evaluating the reusability of as-synthesized Pd NPs. To determine this factor, the Pd-1 and Pd-4 nanocatalysts are used in three cycles for *p*-nitrophenol reduction (Figure 10a−d). The results after the third cycle show a 50% retention of catalytic performance, indicating the reusability of the catalysts.[56] The decrease of catalytic efficiency after the third cycle might be due to the agglomeration and decrease of active sites of the catalysts. It is supported by the PXRD pattern (Figure S5) of the used catalyst, which on analysis reveals that the crystallite size is increased to 8 nm for the used Pd-1 catalyst.

CONCLUSIONS

The present study reveals that the catalytic activity of PVA-embedded Pd nanoparticles toward the reduction of *p*-nitrophenol strictly depends on the size of the metal nanoparticles. The spherical Pd nanocatalyst Pd-1 shows superior catalytic performance toward the reduction of *p*-nitrophenol to *p*-aminophenol by $NaBH_4$ in the green protocol because of its lowest dimension and high surface area compared to the other synthesized nanocatalysts. Besides, metal NPs supported with a relatively lower content of the PVA hydrophilic stabilizer exhibit a temperature-sensitive property. Thus, this strategy provides a new horizon to design a Pd-based temperature-sensitive nanoreactor by using the less expensive polyvinyl alcohol as a capping agent and to find potential application in various biomedical fields, for example, drug delivery systems and sensors.

https://doi.org/10.1021/acsomega.1c00896
ACS Omega 2021, 6, 20746−20757

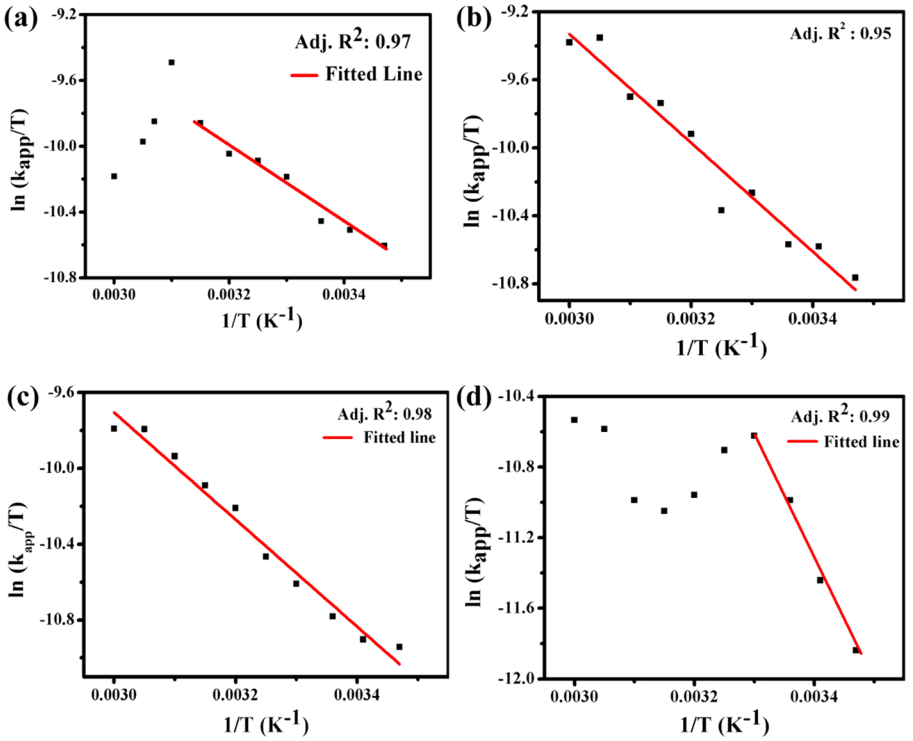

Figure 8. The plot of $\ln(k_{app}/T)$ versus $1/T$ for 4-nitrophenol reduction at different temperatures in the presence of (a) Pd-1, (b) Pd-2, (c) Pd-3, and (d) Pd-4 nanocatalysts. Reaction conditions: [*p*-NP] = 0.133 mM, [$NaBH_4$] = 3.33 mM, and [Pd] = 41.07 × 10^{-7} M.

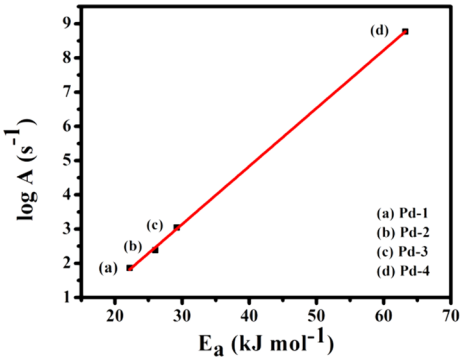

Figure 9. Logarithm of the frequency factor (log *A*) versus apparent activation energy plot of Pd-1, Pd-2, Pd-3, and Pd-4 nanocatalysts toward the reduction of *p*-nitrophenol.

Table 4. Comparison of the Catalytic Performance of the Pd-1 Catalyst with Various Catalysts Reported in the Literature for the Reduction of *p*-Nitrophenol to *p*-Aminophenol by $NaBH_4$

catalysts	k_{app} (×10^3 s^{-1}) at 25 °C	E_{act} (kJ mol^{-1})	reference
Pd-1	8.57	22.2	this work
Pd-GA/RGO	2		[51]
Fe_3O_4@PPy-MAA/Ag	2.38		[52]
Pd_{55}DEN	3.17	31.4	[53]
Pt	0.46 ± 0.06	40	[54]
Cis-AuBP1C-MAM-capped Au NPs	8.9 ± 0.8	35.3 ± 4.0	[13]
Pt@Ag	5.91		[10]
AuAg@pNIPAM@Ag hybrid microgels	8.3		[32]
PdNPs/arabinogalactan polymer	1.83		[55]

EXPERIMENTAL SECTION

General Information. All UV−vis spectra were recorded on a UV-1800 Shimadzu UV−visible spectrophotometer with 1 cm quartz cells. The X-ray diffraction (XRD) patterns were recorded on a Bruker AXS D8 Advance instrument with a Ni-filtered Cu Kα radiation source (λ = 1.5418 Å), operated at 40 kV and 40 mA, employing a scanning rate of 0.2 s/step. FT-IR spectra were determined by using the NICOLET MAGNA IR 750. Scanning electron microscopy (SEM) image measurements were performed under vacuum by using the INSPECT F50 SEM operated at 20.00 kV. Transmission electron microscopy (TEM) measurements were carried out on a Hitachi H 7600 transmission electron microscope.

Materials. Palladium chloride ($PdCl_2$) was obtained from Arora-Matthey, 4-nitrophenol and sodium borohydride were from Sigma-Aldrich, and potassium chloride and polyvinyl alcohol (number average molecular weight: 150,000) were from Merck. The other reagents (AR grade) used in the study were purchased from Merck, India. Moreover, we used Millipore water from Synergy as a solvent for all experiments. In the study, we used all reagents as received without further purification.

Synthesis of PVA-Embedded and Pure Palladium Nanoparticles. In the typical preparation route of Pd-1, initially, 24.5 mL of 1% (w/v) PVA solution was taken in a 100 mL beaker; then, 0.5 mL of an aqueous solution of 0.056 (M) K_2PdCl_4 (2.81 × 10^{-5} mol) was added dropwise into this PVA solution with constant stirring at room temperature. Finally, the whole mixture was continuously stirred with the addition of 8.454 × 10^{-5} mol of $NaBH_4$ for 10 min at 30 °C as shown in our previous work.[3] The yellow color of the aqueous K_2PdCl_4

https://doi.org/10.1021/acsomega.1c00896
ACS Omega 2021, 6, 20746−20757

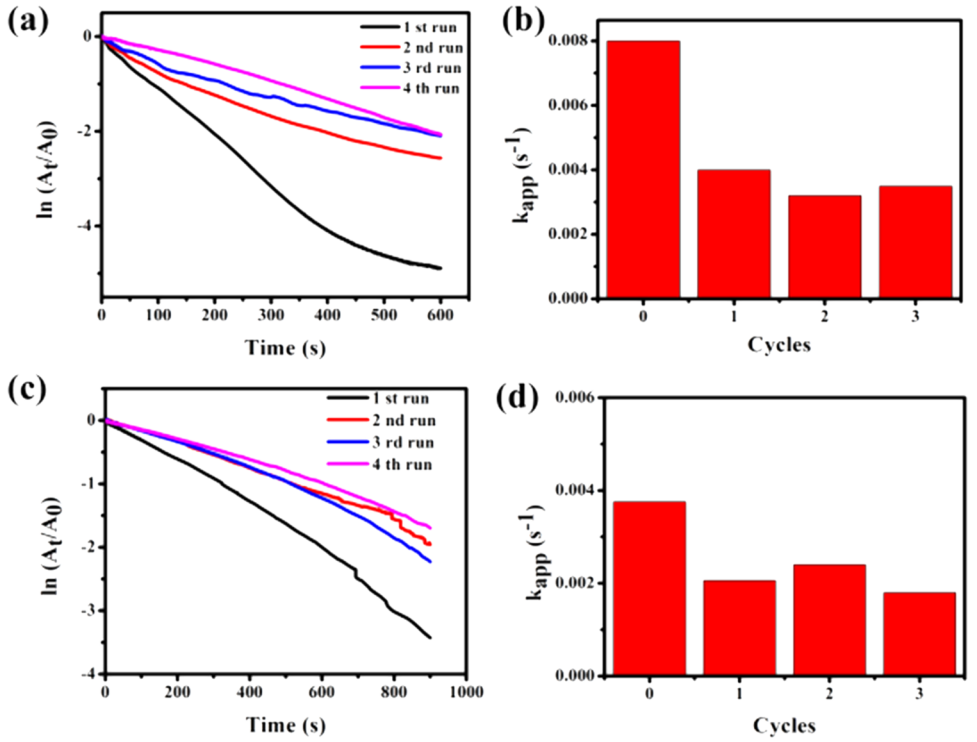

Figure 10. (a) Plots of $\ln(A_t/A_0)$ versus reaction time for the reduction of *p*-nitrophenol by $NaBH_4$ in the presence of the Pd-1 nanocatalyst at 298 K. (b) Plot of rate constants for the reduction of *p*-nitrophenol by the Pd-1 catalyst at different cycles. (c) Plots of $\ln(A_t/A_0)$ versus reaction time for the reduction of *p*-nitrophenol by $NaBH_4$ in the presence of the Pd-4 nanocatalyst at 298 K. (d) Plot of rate constants for the reduction of *p*-nitrophenol by the Pd-4 catalyst at different cycles.

solution changed into grayish black, indicating the formation of Pd(0) NPs. Similarly, for the synthesis of Pd-2, at first, 0.5 mL of 0.056 (M) aqueous K_2PdCl_4 solution (2.81×10^{-5} mol) was added to 24.5 mL of 1% (w/v) PVA solution in a 100 mL beaker at room temperature under constant stirring. Then, 4.225×10^{-5} mol of $NaBH_4$ was mixed with it and stirred for 10 min at 30 °C.

For the synthesis of Pd-3 and Pd-4 catalysts, initially, 5.0 and 1.0 mL of 1% (w/v) PVA solution were taken into two 100 mL beakers separately; then, 0.5 mL of 0.056 (M) aqueous K_2PdCl_4 (2.81×10^{-5} mol) solution was added dropwise into these solutions separately under constant stirring. Then, the total volume of these two solutions was increased to 25 mL by the addition of required volumes of Millipore water. Finally, the whole mixture was stirred continuously with the addition of 8.454×10^{-5} mol of $NaBH_4$ separately for 10 min at 30 °C. The synthesis of pure Pd nanoparticles was done by the same method, only avoiding the use of PVA.

Catalytic Reduction of *p*-Nitrophenol to *p*-Aminophenol by Using Pd Nanocatalysts. Typically, 0.5 mL of 8.0×10^{-4} M *p*-nitrophenol (aqueous solution) was taken in a 4.5 mL quartz cuvette cell with a path length of 1 cm, and 2.14 mL of Millipore water was added to it. Then, 0.35 mL of 0.03 M freshly prepared aqueous solution of $NaBH_4$ was added to the above solution, and the change of color of the solution from light yellow to deep yellow, indicating the formation of *p*-nitrophenolate ion under the alkaline condition, was observed.[37] Immediately after that, 11 μL of 1.127×10^{-3} M Pd NP solution was added to it. Immediately after the addition of catalysts, the time-dependent UV−vis absorption spectra were collected at ambient temperatures.[38] The background correction was done with Millipore water as a reference. The rate constants were determined by measuring the absorbance at 400 nm at different time intervals from the start of the reaction at an ambient temperature. For evaluation of thermodynamics of kinetic parameters, the temperature was altered from 298 to 318 K. The kinetics of the reaction was studied in terms of the Langmuir−Hinshelwood model, and it followed pseudo-first-order with respect to *p*-nitrophenol due to the concentration of $NaBH_4$ is much higher (25 times) compared to that of *p*-nitrophenol. Both the reactants *p*-nitrophenolate from alkaline *p*-nitrophenol and hydrogen from aqueous borohydrides adsorbed on the surface of the Pd NPs before the reaction. For studying the effect of catalyst dose, the amount of the Pd-1 catalyst was varied from 7.47×10^{-7} to 82.13×10^{-7} M in the reaction mixture; however, the volume and concentration of *p*-nitrophenol and $NaBH_4$ were kept constant (0.5 mL of 8.0×10^{-4} M and 0.35 mL of 0.03 M, respectively). Similarly, the *p*-nitrophenol concentration was varied from 0.017 to 0.267 mM, keeping other parameters constant (41.07×10^{-7} M of the Pd-1 catalyst and 0.35 mL of 0.03 M $NaBH_4$), for studying the effect of the concentration of *p*-nitrophenol on the reaction rate. Since the amount of the catalyst in the reaction medium was very low, the recyclability of Pd-1 and Pd-4 catalysts was examined by using 11 μL of 1.127×10^{-3} M Pd catalyst (1.24×10^{-8} mol) in the first run. After virtual completion of the reaction in the first run, 100 μL of 4 mM (0.0004 mmol) *p*-nitrophenol was added to 3 mL of the previous reaction mixture, and the catalytic capability was noted. In this way, the amount of catalysts was kept the same in every cycle. Notably, in the first run, 11 μL of the catalyst was introduced into the solution containing 100 μL of 4 mM (0.0004 mmol) *p*-nitrophenol and 333 μL of 0.03 M (0.010 mmol) sodium borohydride.[10,39]

https://doi.org/10.1021/acsomega.1c00896
ACS Omega 2021, 6, 20746−20757

■ ASSOCIATED CONTENT

Supporting Information

The Supporting Information is available free of charge at https://pubs.acs.org/doi/10.1021/acsomega.1c00896.

The SEM images of Pd-2 and Pd-3 NPs (Figure S1); the particle distribution plots of Pd-1, Pd-2, Pd-3, and Pd-4 from TEM studies (Figure S2); plots of $\ln(A_t/A_0)$ versus reaction time for the reduction of *p*-NP over (a and b) Pd-1, (c) Pd-2, (d) Pd-3, and (e) Pd-4 nanocatalysts at different temperatures (Figure S3); UV−vis spectra of 10 times diluted solution of Pd-1 at different temperatures (Figure S4); the PXRD patterns of used Pd-1 catalyst after the third cycle toward the reduction of *p*-nitrophenol (Figure s5); influence of temperature in the rate constant for the catalytic reduction of *p*-NP by $NaBH_4$ in the presence of Pd-1, Pd-2, Pd-3, and Pd-4 NPs (Table S1); summary of different parameters derived from the fits of the measurement of ln k_{app} versus $1/T$ for the reduction of 4-nitrophenol by using Pd-1, Pd-2, Pd-3, and Pd-4 nanocatalysts (Table S2); and summary of different parameters derived from the fits of the measurement of $\ln(k_{app}/T)$ versus $1/T$ for the reduction of 4-nitrophenol by using Pd-1, Pd-2, Pd-3, and Pd-4 nanocatalysts (Table S3) (PDF)

■ AUTHOR INFORMATION

Corresponding Author

Swapan Kumar Bhattacharya − *Department of Chemistry, Jadavpur University, Kolkata 700032, India;* orcid.org/0000-0002-1218-1860; Phone: 091 9831699643; Email: skbhatt7@yahoo.co.in; Fax: 091 3324146584

Author

Sujit Chatterjee − *Department of Chemistry, Jadavpur University, Kolkata 700032, India*

Complete contact information is available at: https://pubs.acs.org/10.1021/acsomega.1c00896

Author Contributions

S.C.: Conceptualization, formal analysis, investigation, methodology, writing, and editing.

Author Contributions

S.K.B..: Conceptualization, formal analysis, methodology, resources, supervision, writing original draft, review, and editing.

Notes

The authors declare no competing financial interest.

■ ACKNOWLEDGMENTS

We are thankful to Jadavpur University, India, for the financial support and instrumental help.

■ REFERENCES

(1) El-Hout, S. I.; El-Sheikh, S. M.; Hassan, H. M. A.; Harraz, F. A.; Ibrahim, I. A.; El-Sharkawy, E. A. A green chemical route for synthesis of graphene supported palladium nanoparticles: A highly active and recyclable catalyst for reduction of nitrobenzene. *Appl. Catal., A* **2015**, *503*, 176−185.

(2) Roy, P. S.; Bhattacharya, S. K. Size-controlled synthesis and characterization of polyvinyl alcohol-coated platinum nanoparticles: role of particle size and capping polymer on the electrocatalytic activity. *Catal. Sci. Technol.* **2013**, *3*, 1314−1323.

(3) Chatterjee, S.; Bhattacharya, S. K. Size-Dependent Catalytic Activity and Fate of Palladium Nanoparticles in Suzuki−Miyaura Coupling Reactions. *ACS Omega* **2018**, *3*, 12905−12913.

(4) Miyaura, N.; Suzuki, A. Palladium-Catalyzed Cross-Coupling Reactions of Organoboron Compounds. *Chem. Rev.* **1995**, *95*, 2457−2483.

(5) Mahajan, A.; Banik, S.; Roy, P. S.; Roy Chowdhury, S.; Bhattacharya, S. K. Kinetic parameters of anodic oxidation of methanol in alkali: Effect of diameter of Pd nano-catalyst, composition of electrode and solution and mechanism of the reaction. *Int. J. Hydrogen Energy* **2017**, *42*, 21263−21278.

(6) Wu, H.; Zhuo, L.; He, Q.; Liao, X.; Shi, B. Heterogeneous hydrogenation of nitrobenzenes over recyclable Pd(0) nanoparticle catalysts stabilized by polyphenol-grafted collagen fibers. *Appl. Catal., A* **2009**, *366*, 44−56.

(7) Roy, P. S.; Bagchi, J.; Bhattacharya, S. K. Synthesis of polymer-protected palladium nanoparticles of contrasting electrocatalytic activity: A comparative study with respect to reflux time and reducing agents. *Colloids Surf., A* **2010**, *359*, 45−52.

(8) Hu, W.; Wang, H.; Bai, L.; Liu, J.; Luan, X. Pd(0)-Catalyzed Intermolecular Dearomatizing [3 + 2] Spiroannulation of Phenol-Based Biaryls and Allenes. *Org. Lett.* **2018**, *20*, 880−883.

(9) Pandey, S.; Mishra, S. B. Catalytic reduction of p-nitrophenol by using platinum nanoparticles stabilised by guar gum. *Carbohydr. Polym.* **2014**, *113*, 525−531.

(10) Lv, Z.-S.; Zhu, X.-Y.; Meng, H.-B.; Feng, J.-J.; Wang, A.-J. One-pot synthesis of highly branched Pt@Ag core-shell nanoparticles as a recyclable catalyst with dramatically boosting the catalytic performance for 4-nitrophenol reduction. *J. Colloid Interface Sci.* **2019**, *538*, 349−356.

(11) Esumi, K.; Isono, R.; Yoshimura, T. Preparation of PAMAM- and PPI-Metal (Silver, Platinum, and Palladium) Nanocomposites and Their Catalytic Activities for Reduction of 4-Nitrophenol. *Langmuir* **2004**, *20*, 237−243.

(12) Park, S. I.; Song, H.-M. Synthesis of Prolate-Shaped Au Nanoparticles and Au Nanoprisms and Study of Catalytic Reduction Reactions of 4-Nitrophenol. *ACS Omega* **2019**, *4*, 7874−7883.

(13) Lawrence, R. L.; Scola, B.; Li, Y.; Lim, C.-K.; Liu, Y.; Prasad, P. N.; Swihart, M. T.; Knecht, M. R. Remote Optically Controlled Modulation of Catalytic Properties of Nanoparticles through Reconfiguration of the Inorganic/Organic Interface. *ACS Nano* **2016**, *10*, 9470−9477.

(14) Lu, S.; Hu, Y.; Wan, S.; McCaffrey, R.; Jin, Y.; Gu, H.; Zhang, W. Synthesis of Ultrafine and Highly Dispersed Metal Nanoparticles Confined in a Thioether-Containing Covalent Organic Framework and Their Catalytic Applications. *J. Am. Chem. Soc.* **2017**, *139*, 17082−17088.

(15) Veisi, H.; Kazemi, S.; Mohammadi, P.; Safarimehr, P.; Hemmati, S. Catalytic reduction of 4-nitrophenol over Ag nanoparticles immobilized on *Stachys lavandulifolia* extract-modified multi walled carbon nanotubes. *Polyhedron* **2019**, *157*, 232−240.

(16) Li, J.; Liu, C.-y.; Liu, Y. Au/graphene hydrogel: synthesis, characterization and its use for catalytic reduction of 4-nitrophenol. *J. Mater. Chem.* **2012**, *22*, 8426−8430.

(17) Zhao, P.; Feng, X.; Huang, D.; Yang, G.; Astruc, D. Basic concepts and recent advances in nitrophenol reduction by gold- and other transition metal nanoparticles. *Coord. Chem. Rev.* **2015**, *287*, 114−136.

(18) Dong, Z.; Le, X.; Li, X.; Zhang, W.; Dong, C.; Ma, J. Silver nanoparticles immobilized on fibrous nano-silica as highly efficient and recyclable heterogeneous catalyst for reduction of 4-nitrophenol and 2-nitroaniline. *Appl. Catal., B* **2014**, *158-159*, 129−135.

(19) Thawarkar, S. R.; Thombare, B.; Munde, B. S.; Khupse, N. D. Kinetic investigation for the catalytic reduction of nitrophenol using ionic liquid stabilized gold nanoparticles. *RSC Adv.* **2018**, *8*, 38384−38390.

(20) Haldar, K. K.; Kundu, S.; Patra, A. Core-Size-Dependent Catalytic Properties of Bimetallic Au/Ag Core−Shell Nanoparticles. *ACS Appl. Mater. Interfaces* **2014**, *6*, 21946−21953.

(21) Dong, W.; Cheng, S.; Feng, C.; Shang, N.; Gao, S.; Wang, C. Fabrication of highly dispersed Pd nanoparticles supported on reduced graphene oxide for catalytic reduction of 4-nitrophenol. *Catal. Commun.* **2017**, *90*, 70−74.
(22) Aditya, T.; Pal, A.; Pal, T. Nitroarene reduction: a trusted model reaction to test nanoparticle catalysts. *Chem. Commun.* **2015**, *51*, 9410−9431.
(23) Chen, Y.; Wu, T.; Xing, G.; Kou, Y.; Li, B.; Wang, X.; Gao, M.; Chen, L.; Wang, Y.; Yang, J.; Liu, Y.; Zhang, Y.; Wang, D. Fundamental Formation of Three-Dimensional Fe_3O_4 Microcrystals and Practical Application in Anchoring Au as Recoverable Catalyst for Effective Reduction of 4-Nitrophenol. *Ind. Eng. Chem. Res.* **2019**, *58*, 15151−15161.
(24) Sarkar, S.; Sinha, A. K.; Pradhan, M.; Basu, M.; Negishi, Y.; Pal, T. Redox Transmetalation of Prickly Nickel Nanowires for Morphology Controlled Hierarchical Synthesis of Nickel/Gold Nanostructures for Enhanced Catalytic Activity and SERS Responsive Functional Material. *J. Phys. Chem. C* **2011**, *115*, 1659−1673.
(25) Ke, W.; Li, J.; Mohammed, F.; Wang, Y.; Tou, K.; Liu, X.; Wen, P.; Kinoh, H.; Anraku, Y.; Chen, H.; Kataoka, K.; Ge, Z. Therapeutic Polymersome Nanoreactors with Tumor-Specific Activable Cascade Reactions for Cooperative Cancer Therapy. *ACS Nano* **2019**, *13*, 2357−2369.
(26) Lee, J. H.; Bonte, W.; Corthals, S.; Krumeich, F.; Ruitenbeek, M.; van Bokhoven, J. A. Zeolite Nanoreactor for Investigating Sintering Effects of Cobalt-Catalyzed Fischer−Tropsch Synthesis. *Ind. Eng. Chem. Res.* **2019**, *58*, 5140−5145.
(27) Tzounis, L.; Doña, M.; Lopez-Romero, J. M.; Fery, A.; Contreras-Caceres, R. Temperature-Controlled Catalysis by Core−Shell−Satellite AuAg@pNIPAM@Ag Hybrid Microgels: A Highly Efficient Catalytic Thermoresponsive Nanoreactor. *ACS Appl. Mater. Interfaces* **2019**, *11*, 29360−29372.
(28) Anderson, A. M.; Nguyen, M. L.; Potter, M.; Rosario, D.; Kempinska, K.; Ellis, R. J.; Diccianni, M.; Letendre, S. L. Comparison of bead array and glass nanoreactor multi-analyte platforms for the evaluation of CNS and peripheral inflammatory markers during HIV infection. *J. Immunol. Methods* **2019**, *465*, 7−12.
(29) Poupart, R.; Benlahoues, A.; Le Droumaguet, B.; Grande, D. Porous Gold Nanoparticle-Decorated Nanoreactors Prepared from Smartly Designed Functional Polystyrene-block-Poly(D,L-Lactide) Diblock Copolymers: Toward Efficient Systems for Catalytic Cascade Reaction Processes. *ACS Appl. Mater. Interfaces* **2017**, *9*, 31279−31290.
(30) Acosta, B.; Evangelista, V.; Miridonov, S.; Fuentes, S.; Simakov, A. The Decoration of Gold Core in Au@ZrO_2 Nanoreactors with Trace Amounts of Pd for the Effective Reduction of 4-Nitrophenol to 4-Aminophenol. *Catal. Lett.* **2019**, *149*, 1621−1632.
(31) Zhang, J.-T.; Bhat, R.; Jandt, K. D. Temperature-sensitive PVA/PNIPAAm semi-IPN hydrogels with enhanced responsive properties. *Acta Biomater.* **2009**, *5*, 488−497.
(32) Liu, B.; Yu, S.; Wang, Q.; Hu, W.; Jing, P.; Liu, Y.; Jia, W.; Liu, Y.; Liu, L.; Zhang, J. Hollow mesoporous ceria nanoreactors with enhanced activity and stability for catalytic application. *Chem. Commun.* **2013**, *49*, 3757−3759.
(33) Begum, R.; Farooqi, Z. H.; Butt, Z.; Wu, Q.; Wu, W.; Irfan, A. Engineering of responsive polymer based nano-reactors for facile mass transport and enhanced catalytic degradation of 4-nitrophenol. *J. Environ. Sci.* **2018**, *72*, 43−52.
(34) Liu, J.; Li, J.; Meng, R.; Jian, P.; Wang, L. Silver nanoparticles-decorated-Co_3O_4 porous sheets as efficient catalysts for the liquid-phase hydrogenation reduction of p-Nitrophenol. *J. Colloid Interface Sci.* **2019**, *551*, 261−269.
(35) Neal, R. D.; Inoue, Y.; Hughes, R. A.; Neretina, S. Catalytic Reduction of 4-Nitrophenol by Gold Catalysts: The Influence of Borohydride Concentration on the Induction Time. *J. Phys. Chem. C* **2019**, *123*, 12894−12901.
(36) Wang, P.; Zhang, M.; Cai, Y. T.; Cai, S. Y.; Du, M. L.; Zhu, H.; Bao, S. Y.; Xie, Q. Facile Fabrication of Palladium Nanoparticles Immobilized on the Water-Stable Polyvinyl Alcohol/Polyehylenei-mine Nanofibers Via *In-Situ* Reduction and Their High Electrochemical Activity. *Soft Matter* **2014**, *12*, 387−395.
(37) Wang, Y.; Li, Q.; Zhang, P.; O'Connor, D.; Varma, R. S.; Yu, M.; Hou, D. One-pot green synthesis of bimetallic hollow palladium-platinum nanotubes for enhanced catalytic reduction of p-nitrophenol. *J. Colloid Interface Sci.* **2019**, *539*, 161−167.
(38) Lin, F.-h.; Doong, R.-a. Bifunctional Au−Fe_3O_4 Heterostructures for Magnetically Recyclable Catalysis of Nitrophenol Reduction. *J. Phys. Chem. C* **2011**, *115*, 6591−6598.
(39) Wu, G.; Liang, X.; Zhang, L.; Tang, Z.; Al-Mamun, M.; Zhao, H.; Su, X. Fabrication of highly stable metal oxide hollow nanospheres and their catalytic activity toward 4-nitrophenol reduction. *ACS Appl. Mater. Interfaces* **2017**, *9*, 18207−18214.
(40) Gu, S.; Wunder, S.; Lu, Y.; Ballauff, M.; Fenger, R.; Rademann, K.; Jaquet, B.; Zaccone, A. Kinetic Analysis of the Catalytic Reduction of 4-Nitrophenol by Metallic Nanoparticles. *J. Phys. Chem. C* **2014**, *118*, 18618−18625.
(41) Gkizis, P. L.; Stratakis, M.; Lykakis, I. N. Catalytic activation of hydrazine hydrate by gold nanoparticles: Chemoselective reduction of nitro compounds into amines. *Catal. Commun.* **2013**, *36*, 48−51.
(42) Liu, L.; Chen, R.; Liu, W.; Wu, J.; Gao, D. Catalytic reduction of 4-nitrophenol over Ni-Pd nanodimers supported on nitrogen-doped reduced graphene oxide. *J. Hazard. Mater.* **2016**, *320*, 96−104.
(43) Imura, Y.; Tsujimoto, K.; Morita, C.; Kawai, T. Preparation and Catalytic Activity of Pd and Bimetallic Pd−Ni Nanowires. *Langmuir* **2014**, *30*, 5026−5030.
(44) Johnson, J. A.; Makis, J. J.; Marvin, K. A.; Rodenbusch, S. E.; Stevenson, K. J. Size-Dependent Hydrogenation of p-Nitrophenol with Pd Nanoparticles Synthesized with Poly(amido)amine Dendrimer Templates. *J. Phys. Chem. C* **2013**, *117*, 22644−22651.
(45) Kästner, C.; Thünemann, A. F. Catalytic Reduction of 4-Nitrophenol Using Silver Nanoparticles with Adjustable Activity. *Langmuir* **2016**, *32*, 7383−7391.
(46) Gu, X.; Qi, W.; Xu, X.; Sun, Z.; Zhang, L.; Liu, W.; Pan, X.; Su, D. Covalently functionalized carbon nanotube supported Pd nanoparticles for catalytic reduction of 4-nitrophenol. *Nanoscale* **2014**, *6*, 6609−6616.
(47) Cui, K.; Zhong, W.; Li, L.; Zhuang, Z.; Li, L.; Bi, J.; Yu, Y. Well-Defined Metal Nanoparticles@Covalent Organic Framework Yolk−Shell Nanocages by ZIF-8 Template as Catalytic Nanoreactors. *Small* **2018**, *15*, 1804419.
(48) Hervés, P.; Pérez-Lorenzo, M.; Liz-Marzán, L. M.; Dzubiella, J.; Lu, Y.; Ballauff, M. Catalysis by metallic nanoparticles in aqueous solution: model reactions. *Chem. Soc. Rev.* **2012**, *41*, 5577−5587.
(49) Chen, X.; Cai, Z.; Chen, X.; Oyama, M. AuPd bimetallic nanoparticles decorated on graphene nanosheets: their green synthesis, growth mechanism and high catalytic ability in 4-nitrophenol reduction. *J. Mater. Chem. A* **2014**, *2*, 5668−5674.
(50) Kumar, M.; Deka, S. Multiply Twinned AgNi Alloy Nanoparticles as Highly Active Catalyst for Multiple Reduction and Degradation Reactions. *ACS Appl. Mater. Interfaces* **2014**, *6*, 16071−16081.
(51) Vilian, A. T. E.; Choe, S. R.; Giribabu, K.; Jang, S.-C.; Roh, C.; Huh, Y. S.; Han, Y.-K. Pd nanospheres decorated reduced graphene oxide with multi-functions: Highly efficient catalytic reduction and ultrasensitive sensing of hazardous 4-nitrophenol pollutant. *J. Hazard. Mater.* **2017**, *333*, 54−62.
(52) Das, R.; Sypu, V. S.; Paumo, H. K.; Bhaumik, M.; Maharaj, V.; Maity, A. Silver decorated magnetic nanocomposite (Fe_3O_4@PPy-MAA/Ag) as highly active catalyst towards reduction of 4-nitrophenol and toxic organic dyes. *Appl. Catal., B* **2019**, *244*, 546−558.
(53) Bingwa, N.; Meijboom, R. Kinetic Evaluation of Dendrimer-Encapsulated Palladium Nanoparticles in the 4-Nitrophenol Reduction Reaction. *J. Phys. Chem. C* **2014**, *118*, 19849−19858.
(54) Wunder, S.; Polzer, F.; Lu, Y.; Mei, Y.; Ballauff, M. Kinetic Analysis of Catalytic Reduction of 4-Nitrophenol by Metallic Nanoparticles Immobilized in Spherical Polyelectrolyte Brushes. *J. Phys. Chem. C* **2010**, *114*, 8814−8820.

https://doi.org/10.1021/acsomega.1c00896
ACS Omega 2021, 6, 20746−20757

(55) Kora, A. J.; Rastogi, L. Green synthesis of palladium nanoparticles using gum ghatti (*Anogeissus latifolia*) and its application as an antioxidant and catalyst. *Arabian J. Chem.* **2018**, *11*, 1097−1106.
(56) Al-Namil, D. S.; El Khoury, E.; Patra, D. Solid-State Green Synthesis of Ag NPs: Higher Temperature Harvests Larger Ag NPs but Smaller Size Has Better Catalytic Reduction Reaction. *Sci. Rep.* **2019**, *9*, 15212−15219.

https://doi.org/10.1021/acsomega.1c00896
ACS Omega 2021, 6, 20746−20757